Optimal work-to-work conversion of a nonlinear quantum Brownian duet

Matteo Carrega,[1,*] Maura Sassetti,[2,3] and Ulrich Weiss[4]
[1]*NEST, Istituto Nanoscienze-CNR and Scuola Normale Superiore, I-56127 Pisa, Italy*
[2]*Dipartimento di Fisica, Università di Genova, Via Dodecaneso 33, 16146 Genova, Italy*
[3]*SPIN-CNR, Via Dodecaneso 33, 16146 Genova, Italy*
[4]*II. Institut für Theoretische Physik, Universität Stuttgart, D-70550 Stuttgart, Germany*

(Received 30 January 2019; revised manuscript received 9 April 2019; published 18 June 2019)

Performances of work-to-work conversion are studied for a dissipative nonlinear quantum system with two isochromatic phase-shifted drives. It is shown that for weak Ohmic damping simultaneous maximization of efficiency with finite power yield and low power fluctuations can be achieved. Optimal performances of these three quantities are accompanied by a shortfall of the tradeoff bound recently introduced for classical thermal machines. This bound can be undercut down to zero for sufficiently low temperature and weak dissipation, where the non-Markovian quantum nature dominates. Analytic results are given for linear thermodynamics. These general features can persist in the nonlinear driving regime near a maximum of the power yield and a minimum of the power fluctuations. This broadens the scope to an operation field beyond linear response.

DOI: 10.1103/PhysRevA.99.062111

I. INTRODUCTION

Major efforts in classical and quantum thermodynamics are directed at strategies to efficiently manipulate and transform varied forms of energy into useful ones [1–11]. Optimal heat-to-work conversion is a founding principle for a wide range of applications, from industrial processes to biological functionalities, thermoelectricity, and photovoltaics [3]. The seminal work of Carnot established an upper bound, $\eta \leqslant \eta_C$, for the efficiency η of all heat engines. It is argued that this bound is saturated for reversible operation with vanishing power yield [3,12–16]. This poses a severe restriction, as finite power output is essential for usable thermal machines. However, both efficiency and yield have to be sufficiently large for a well working engine: if η is small, a major part of energy is wasted, while low output power would not supply sizable work in finite time. Various studies focused on the maximum attainable efficiency at a given finite power yield [17–21]. General relations linking maximum power, maximum efficiency, and minimum dissipation have been derived within linear thermodynamics [22–26]. It has been proposed that constraints on efficiency at finite power could be overcome in specific settings, e.g., by breaking time-reversal symmetry [22]. Various attempts to get close to Carnot efficiency upon retaining finite power have been made [27–30], e.g., by suggesting working points near critical phase transitions [28,29]. However, these settings are impaired by large power fluctuations, which undermine effective working of the machine [29,31].

A universal tradeoff criterion, a bound constraining these quantities and holding for a wide class of classical Markovian systems operating in the steady state, has been derived [32–37]. The bound implies that high power yield, efficiency close to the Carnot value, and small power fluctuations are not compatible. Generalizations of the tradeoff bound holding for time-periodic systems have been discussed [38,39]. Recently, weakening of the tradeoff bound has been found in ballistic multiterminal transport [40] and in coherent electron transport through resonant single- and double-dot junctions without [41] and with electron interactions [42].

It is therefore interesting to study systematically the impact of quantum effects on the tradeoff criterion in a key model of quantum transport: a quantum Brownian particle (QBP) moving in a tight-binding (TB) lattice and coupled to a thermal reservoir creating Ohmic friction. With two time-dependent external drives, the system forms a quantum Brownian duet and acts as an isothermal work-to-work converter. The QBP model has widely varied applications [43]. It describes, e.g., the current-voltage characteristics of a Josephson junction [44–46], transport of charge through impurities in quantum wires [47,48], and tunneling of edge currents through constrictions in one-dimensional interacting fermion systems [49–53]. The Ohmic spectral coupling entails power laws for the temperature and bias dependence of tunneling rates. This leads for weak damping, e.g., to increasing tunneling with decreasing temperature [54,55].

In this paper we first show within linear thermodynamics and weak tunneling, that the specific Ohmic features make it possible to optimize performance upon simultaneous adjustment of large power yield, high efficiency, and low power fluctuations. We find that for weak damping the tradeoff quantity can fall below the classical bound and can even approach zero, as temperature is decreased and the non-Markovian quantum regime is reached. We also focus on a hitherto mostly disregarded regime beyond linear thermodynamics, in which nonlinear external driving and response prevails. We there discover a parameter regime with sizable power yield, low power fluctuations, and efficiency still close to unity.

*matteo.carrega@nano.cnr.it

II. MODEL

Consider a quantum Brownian particle (QBP) in a tight-binding (TB) lattice bilinearly coupled to a thermal bath of harmonic oscillators at inverse temperature β. The TB Hamiltonian is $H_{\rm TB} = -\frac{1}{2}\hbar\Delta\sum_n (a_n^\dagger a_{n+1} + {\rm H.c.})$ and the bath-plus-coupling term is $H_{\rm RI} = \sum_\alpha [\frac{p_\alpha^2}{2m_\alpha} + \frac{m_\alpha\omega_\alpha^2}{2}(x_\alpha - \frac{c_\alpha}{m_\alpha\omega_\alpha}q)^2]$, where $q = q_0\sum_n a_n^\dagger a_n$, and q_0 is the lattice constant. The spectral bath coupling is $J(\omega) = \frac{\pi}{2}\sum_\alpha \frac{c_\alpha^2}{m_\alpha\omega_\alpha}\delta(\omega - \omega_\alpha)$ [43,56]. In the Ohmic scaling limit we have $J(\omega) = 2\pi K\omega$, where K is the dimensionless damping strength. The bare transfer amplitude Δ is adiabatically renormalized by the modes $\omega > \omega_{\rm c}$ to the dressed amplitude $\Delta_{\rm r} = \Delta(\Delta/\omega_{\rm c})^{K/(1-K)}$. The QBP model maps *inter alia* on quasiparticles tunneling through a quantum point contact (QPC) in the fractional quantum Hall (FQH) regime [49,50], whereby K corresponds to the fractional filling factor ν. The weak-damping regime $K \ll 1$ matches up with strong repulsive short-range electron interactions.

Here we study energy input and output of the single-band QBP model under time-periodic drive $H_{\rm ext}(t) = -\hbar\epsilon(t)\,q/q_0$, where $\epsilon(t) = \epsilon(t+\mathcal{T})$. When the QBP is subjected to two independent drives, $\epsilon(t) = \epsilon_1(t) + \epsilon_2(t)$, as discussed for a classical setting in Refs. [23,25], it can operate as a work-to-work converter. But it will require that the respective work rates or powers, $\dot{W}_i \equiv P_i(t) = \epsilon_i(t)\dot{q}(t)$, $i = 1, 2$, can be distinguished. We now choose $\hbar = k_{\rm B} = q_0 = 1$.

At long times, the power $P_i(t)$ reaches the periodic state $\overline{P}_i(t) = \overline{P}_i(t+\mathcal{T})$, and the mean power is $\langle P_i\rangle = \int_0^{\mathcal{T}} dt\,\overline{P}_i(t)/\mathcal{T}$. With the deviation $\delta P_i(t) = P_i(t) - \overline{P}_i(t)$, the power fluctuations are $\overline{D}_i(t) = \int_0^t dt' \int_0^t dt''\,\overline{\delta P_i(t')\delta P_i(t'')}/t$, and the mean power spread is $\langle D_i\rangle = \int_0^{\mathcal{T}} dt\,\overline{D}_i(t)/\mathcal{T}$.

Consider now mean power and power fluctuations of the driven QBP. First, we deal with order Δ^2, which is the leading contribution in the weak-tunneling regime. It describes transport via nearest-neighbor transitions, and single-electron transport in the related fermionic model. We have (see Appendix)

$$\langle P_i\rangle = \int_0^\infty d\tau\, k_{\rm P}(\tau)\int_0^{\mathcal{T}}\frac{dt}{\mathcal{T}}\,\epsilon_i(t)\sin[G(t,t-\tau)], \tag{1}$$

$$\langle D_i\rangle = \int_0^\infty d\tau\, k_D(\tau)\int_0^{\mathcal{T}}\frac{dt}{\mathcal{T}}\,\epsilon_i(t)\epsilon_i(t-\tau)\cos[G(t,t-\tau)], \tag{2}$$

with $G(t_2,t_1) = \int_{t_1}^{t_2} dt'\,[\epsilon_1(t') + \epsilon_2(t')]$. The functions $k_{\rm P/D}(\tau)$ carry the amplitude factor $\Delta_{\rm r}^{2-2K}$ and the Ohmic bath correlations. They read $k_{\rm D}(\tau) = \cot(\pi K)k_{\rm P}(\tau)$ and [43,56,57]

$$k_{\rm P}(\tau) = \Delta_{\rm r}^2\left(\frac{\pi}{\beta\Delta_{\rm r}}\right)^{2K}\frac{\sin(\pi K)}{\sinh(\pi\tau/\beta)^{2K}}. \tag{3}$$

When the mean powers have opposite sign, $\langle P_1\rangle\langle P_2\rangle < 0$, the QBP entity is acting as work-to-work converter with the positive power being the input and the negative power being the output or yield [1,25]. If $\langle P_2\rangle$ is the input and $\langle P_1\rangle$ is the yield, the efficiency of the converter is $\eta \equiv |\langle P_1\rangle|/\langle P_2\rangle \leqslant 1$. Optimal performance is characterized by maximal efficiency at given input. However, optimization of the converter should also conform to power fluctuations as low as possible. The latter may be rated with the estimate of relative uncertainty

$$\Sigma_1 = \sqrt{\langle D_1\rangle/\langle P_1\rangle^2}. \tag{4}$$

It has been argued and proved for a huge class of steady-state heat engines with internal classical states that there is a tradeoff between large power, high efficiency, and low relative uncertainty, being expressed by the joint bound [32–35,37]

$$Q_1 \equiv \beta|\langle P_1\rangle|(1/\eta - 1)\Sigma_1^2 \geqslant 2. \tag{5}$$

If efficiency is close to unity with considerable yield, the bound implies that the power fluctuations are quite large. Conversely, if the bound is broken, simultaneous attainment of maximal efficiency, sizable yield, and low power fluctuations is within reach. This can happen indeed, as shown below.

III. WORK-TO-WORK CONVERSION WITH TWO MONOCHROMATIC DRIVES

If the frequencies of the two drives would be different, the work rates could clearly be distinguished. But here we choose the same frequency. Otherwise, the single-band model could not operate as a converter in the linear regime, as different frequencies would not couple [24]. We put

$$\begin{aligned}\epsilon_1(t) &= F_1\sin(\omega t),\\ \epsilon_2(t) &= F_2\cos(\omega t - \varphi).\end{aligned} \tag{6}$$

Here, the tunable phase shift $\varphi = \arctan\alpha$ determines the (time-reversal) asymmetry between the two drives.

The drives (6) can be combined into

$$\begin{aligned}\epsilon(t) &= \mathcal{F}\sin(\omega t + \Phi),\\ \mathcal{F} &= {\rm sgn}\,(F_1 + F_2\sin\varphi)\big[F_1^2 + F_2^2 + 2F_1F_2\sin\varphi\big]^{1/2},\\ \Phi &= \arctan[F_2\cos\varphi/(F_1 + F_2\sin\varphi)].\end{aligned} \tag{7}$$

With (6) and (7) the time-averaged powers are found as (see Appendix)

$$\begin{aligned}\langle P_1\rangle &= \int_0^\infty d\tau\, k_{\rm P}(\tau)\,F_1\,J_1[A(\tau)]\cos(\Phi - \omega\tau/2),\\ \langle P_2\rangle &= \int_0^\infty d\tau\, k_{\rm P}(\tau)\,F_2\,J_1[A(\tau)]\sin(\Phi + \varphi - \omega\tau/2)\end{aligned} \tag{8}$$

with $A(\tau) = 2\mathcal{F}\sin(\omega\tau/2)/\omega$, and $J_n(z)$ is a Bessel function. The mean power fluctuations are found from Eq. (2) as

$$\begin{aligned}\langle D_i\rangle &= \frac{1}{2}\int_0^\infty d\tau\, k_{\rm D}(\tau)\,d_i(\tau), \quad i = 1, 2,\\ d_1(\tau) &= F_1^2\{J_0[A(\tau)]\cos(\omega\tau) - J_2[A(\tau)]\cos(2\Phi)\},\\ d_2(\tau) &= F_2^2\{J_0[A(\tau)]\cos(\omega\tau) + J_2[A(\tau)]\cos(2\Phi + 2\varphi)\}.\end{aligned} \tag{9}$$

The expressions (8) and (9) are exact in the weak-tunneling limit for arbitrary strength of the driving amplitudes F_1 and F_2.

As the drives (6) have common frequency, one may question whether the powers (8) and fluctuations (9) can be experimentally distinguished. This is possible, in fact, when the forces (6) are independent, e.g., when they operate spatially

separated. A system which can be mapped on the driven QBP is a quantum point contact (QPC) in a fractional quantum Hall (FQH) bar [49,50,58–61] with two spatially separated terminals at which the gate voltage drives are applied. The filling factor ν corresponds to the Ohmic coupling parameter K. In such a physical implementation, the powers (8), and power fluctuations (9) can be measured individually. The QPC model with mapping on the QBP is discussed in the Appendix.

A. Linear response

In the linear response (LR) regime, the dependence of the mean powers on the driving amplitudes F_1 and F_2 is expressed in terms of the Onsager matrix $\mathcal{L}$ as $\langle P_i\rangle = F_i \sum_{j=1,2} \mathcal{L}_{i,j} F_j$. We get from Eqs. (8)

$$\mathcal{L} = L_{\rm s}(\omega)\begin{pmatrix} 1 & \frac{\alpha+\kappa}{\sqrt{1+\alpha^2}} \\ \frac{\alpha-\kappa}{\sqrt{1+\alpha^2}} & 1 \end{pmatrix}, \tag{10}$$

where $\kappa = L_{\rm c}(\omega)/L_{\rm s}(\omega)$, and where

$$L_{\rm s}(\omega) = \frac{1}{2\omega}\int_0^\infty d\tau\, k_{\rm P}(\tau)\sin(\omega\tau),$$
$$L_{\rm c}(\omega) = \frac{1}{2\omega}\int_0^\infty d\tau\, k_{\rm P}(\tau)[1-\cos(\omega\tau)]. \tag{11}$$

The functions $L_{\rm s}(\omega)$ and κ bear Ohmic bath correlations. Dependence on β, ω, and K can be given in analytic form (see Appendix). The parameter α controls the phase shift of the drive (6). In addition, in the LR regime the power variance becomes $\langle D_i\rangle = F_i^2\omega\coth(\beta\omega/2)L_{\rm s}(\omega)$ (see Appendix).

The Onsager matrix conveys the interplay of phase tuning of the driving forces and exchange of energy ω between bath and QBP. In the limit $\alpha\to\infty$ ($\varphi\to\pi/2$), the Onsager matrix is symmetric, and the work-to-work converter operates time-reversal symmetrically. As α is lowered, the Onsager matrix gets antisymmetric admixtures, and time-reversal symmetry is broken. In our setting, this scenario sets in without switching on external magnetic fields [22]. In the limit $\alpha\to 0$ ($\varphi\to 0$), the Onsager matrix is antisymmetric. Upon tuning α, one moves forth or back between these limiting cases.

For the linear model (10), the maximum output power is at $F_1 = F_{1,\rm MP} \equiv -(\alpha+\kappa)F_2/(2\sqrt{1+\alpha^2})$:

$$\langle P_{1,\rm MP}\rangle \equiv \langle P_1(F_{1,\rm MP},F_2)\rangle = -L_{\rm s}(\omega)\,F_{1,\rm MP}^2. \tag{12}$$

The condition $\langle P_1(F_1,F_2)\rangle/\langle P_{1,\rm MP}\rangle = P^\star$ has two roots, which are $F_{1,\pm} = (1\pm\sqrt{1-P^\star})\,F_{1,\rm MP}$. Correspondingly, efficiency and power fluctuations as functions of $P^\star$ have two branches,

$$\eta_\pm = \frac{P^*}{2}\frac{X}{1+2/Y\mp\sqrt{1-P^*}}, \tag{13}$$

$$\Sigma_{1,\pm} = \frac{2}{F_2}\frac{\sqrt{1+\alpha^2}}{\alpha+\kappa}\sqrt{\frac{\omega\coth(\beta\omega/2)}{L_{\rm s}(\omega)}}\frac{1\pm\sqrt{1-P^*}}{P^*}, \tag{14}$$

where $X = (\alpha+\kappa)/(\alpha-\kappa)$ and $Y = (\alpha^2-\kappa^2)/(1+\kappa^2)$. The respective two branches collide at $P^\star = 1$.

The two branches are plotted versus $P^\star$ in Fig. 1 for efficiency (left) and power fluctuations (right). The behaviors are qualitatively different for $\alpha>\kappa$ and $\alpha<\kappa$. The left panel shows that high efficiency can be reached on the (+) branch when $\alpha>\kappa$, and on the (−) branch when $\alpha<\kappa$. In contrast, low power fluctuations arise only in branch (−) when $\alpha<\kappa$. Hence high efficiency is compatible with low power fluctuations when $\alpha<\kappa$, i.e., when the antisymmetric off-diagonal parts of the Onsager matrix outweigh the symmetric ones.

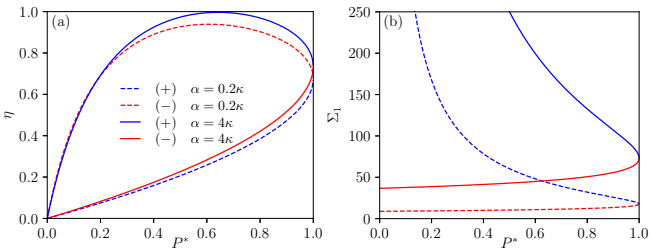

FIG. 1. Efficiency (a) and power fluctuations (b) in the LR regime as function of P^* (see text). Blue (red) color refers to the + (−) branch. The solid curve is $\alpha = 4\kappa$ and the dashed curve $\alpha = 0.2\kappa$. Other parameters are $\beta\omega = 6$, $\omega = 5\,\Delta_{\rm r}$, $\Delta_{\rm r} = 1$, $K = 0.1$, and $F_2 = 0.1\omega$.

To find optimum working conditions, we now focus on the maximum efficiency (ME) at notable power yield. The efficiency $\eta(F_1)$ for fixed F_2 is maximal at $F_1 = F_{1,\rm ME}$, where $F_{1,\rm ME} = -F_2(\sqrt{1+\kappa^2}-\sqrt{1+\alpha^2})/(\kappa-\alpha)$, and is given by

$$\eta_{\rm ME} = \frac{\sqrt{1+\alpha^2}-\sqrt{1+\kappa^2}}{\sqrt{1+\alpha^2}+\sqrt{1+\kappa^2}}\frac{\alpha+\kappa}{\alpha-\kappa}. \tag{15}$$

Figure 2(a) shows $\eta_{\rm ME}$ versus $\beta\omega$ for different interaction strengths K. As K is decreased, $\eta_{\rm ME}$ is strictly increasing. In the asymptotic non-Markovian low temperature regime $\beta\omega\gg 1$, in which [62]

$$\kappa(\beta\omega)\to\tan(\pi K)[(\beta\omega/(2\pi))^{1-2K}\Gamma(K)^2/\pi - 1], \tag{16}$$

the function $\kappa(\beta\omega)$ diverges as $(\beta\omega)^{1-2K}$ for $0<K<1/2$ and is a positive constant for $1/2<K<1$. Hence, as $\beta\omega\to\infty$, $\eta_{\rm ME}$ reaches unity in the former case and a value less than unity in the latter case. For $K\ll 1/2$, the prefactor of the term $(\beta\omega/(2\pi))^{1-2K}$ in Eq. (16) is π/K. Thus, for weak Ohmic damping, or large repulsive Coulomb interaction in the associated fermionic transport model, the ME efficiency dwells close to unity in a considerably wide temperature range.

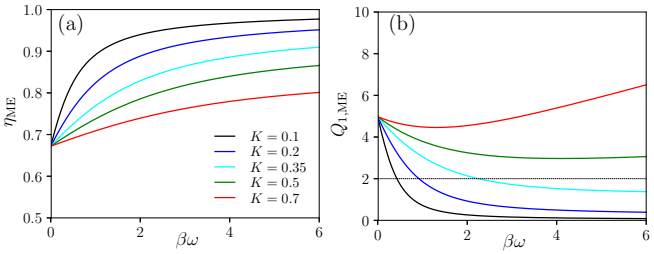

FIG. 2. Maximum efficiency $\eta_{\rm ME}$ (a) and tradeoff criterion $Q_{1,\rm ME}$ (b) versus $\beta\omega$ in the LR regime for $\alpha = 5$ and different K [in both (a) and (b)]. See text. Shortfall of the bound 2 occurs for $K\lessapprox 0.4$. The gradual increase of $Q_{1,\rm ME}$ in the range $1/4<K\lessapprox 0.4$ takes place at higher $\beta\omega$ than shown in (b).

Eventually, with the function $c(x) = 2x\coth(x/2)$, the tradeoff criterion (5) at $F_1 = F_{1,\mathrm{ME}}$ takes the concise form (see Appendix)

$$Q_{1,\mathrm{ME}} = c(\beta\omega)\frac{\sqrt{1+\alpha^2}}{(\alpha+\kappa)^2}\left(\frac{1-\alpha\kappa}{\sqrt{1+\kappa^2}} + \sqrt{1+\alpha^2}\right). \quad (17)$$

In Fig. 2(b) the quantity $Q_{1,\mathrm{ME}}$ is plotted versus $\beta\omega$ for different values of K. Since $\kappa(\beta\omega \to 0, K) \to 0$, the curves start out for all K at the value $4\sqrt{1+\alpha^2}(1+\sqrt{1+\alpha^2})/\alpha^2$. In the regime $1/2 < K < 1$, we have $\kappa(\beta\omega \to \infty) = -\tan(\pi K)$, and hence $Q_{1,\mathrm{ME}}$ grows linearly with inverse temperature at low temperatures, whereas $|\langle P_{1,\mathrm{ME}}\rangle|$ and $\Sigma_{1,\mathrm{ME}}$ become constant in this limit. In contrast, in the range $0 < K < 1/2$, $\kappa(\beta\omega \to \infty)$ diverges asymptotically as $(\beta\omega)^{1-2K}$. Thus, the power $|\langle P_{1,\mathrm{ME}}\rangle|$ grows as $(\beta\omega)^{1-2K}$, the relative uncertainty $\Sigma_{1,\mathrm{ME}}$ drops to zero as $(\beta\omega)^{2K-1}$, and the quantity $Q_{1,\mathrm{ME}}$ varies as $(\beta\omega)^{4K-1}$ in this limit. As a result, $Q_{1,\mathrm{ME}}$ diverges in the range $1/4 < K < 1/2$, stays flat below 2 for $K = 1/4$, and drops to zero when K is in the range $0 < K < 1/4$, as $\beta\omega \to \infty$. Hence the QBP work converter has optimal performance for weak damping $0 < K < 1/4$. With decreasing temperature the quantity $Q_{1,\mathrm{ME}}$ falls well below the classical bound 2, and eventually drops to zero, as the non-Markovian quantum regime is reached. Hence large power, high efficiency, and small power fluctuations are in fact compatible.

We have investigated the impact of an additional n-fold frequency drive in the output, $\epsilon_1(t) = F_1[\sin(\omega t + \gamma_n \sin(n\omega t)]$. We found that the behaviors shown in Figs. 1 and 2 change only marginally for $0 < \gamma_n < 1$. Details are given in the Appendix.

B. Nonlinear response

The above results of the LR regime hold when the driving amplitude F_2 is sufficiently small, $F_2 \ll \alpha\omega$. For larger F_2, the interplay of nonlinear driving with bath correlations becomes significant, and the ME analysis must start with the original expressions (8) and (9). The ME point $F_1 = F_{1,\mathrm{ME}}$ is found as the numerical root of $d\eta/dF_1 = 0$. With this, numerical nonlinear response (NLR) computation of $P_{1,\mathrm{ME}}$, $\eta_{1,\mathrm{ME}}$, $\Sigma_{1,\mathrm{ME}}$, and $Q_{1,\mathrm{ME}}$ is straightforward.

The characteristic behaviors of $\langle P_{1,\mathrm{ME}}\rangle$, $\eta_{1,\mathrm{ME}}$, and $\Sigma_{1,\mathrm{ME}}$ versus F_2/ω in the NLR are shown in Figs. 3(a)–3(c) for $\beta\omega = 6$ (blue) and $\beta\omega = 2$ (red) for $K = 0.1$. Clear deviations from the LR behaviors occur in (a), (b), and (c), as F_2/ω is increased. The yield $|\langle P_{1,\mathrm{ME}}\rangle|$ reaches a maximum near $F_2/\omega = 7.5$ for both temperatures. By contrast, the NLR power fluctuations run through a flat minimum located near $F_2/\omega = 2$ for $\beta\omega = 6$ and near $F_2/\omega = 4$ for $\beta\omega = 2$ and spanning a broad amplitude range. In this area, the work-to-work converter has sizable power yield with simultaneous low power fluctuations and efficiency still close to unity, only slightly smaller than in LR. This indicates that the NLR regime is a promising field for finding the best compromise between large power yield, low power fluctuations and high efficiency. Panel (d) displays the tradeoff criterion $Q_{1,\mathrm{ME}}$ versus $\beta\omega$ for different values of F_2/ω. Most interestingly, the quantity $Q_{1,\mathrm{ME}}$ falls below 2 for F_2/ω below 5.5 and sufficiently low temperature. In contrast, it consistently stays above 2 for larger F_2/ω and arbitrarily low temperatures. In the former case, the power fluctuations are in the flat minimum of panel (b), thereby facilitating shortfall of the tradeoff bound in the NLR.

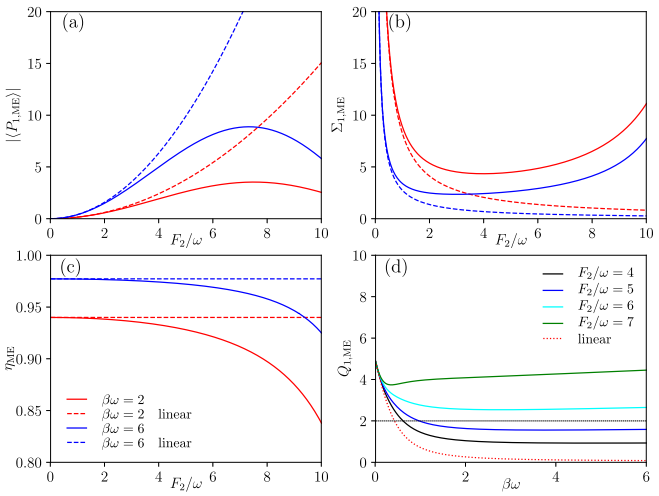

FIG. 3. Nonlinear regime. (a) and (b) Mean power and power fluctuations at maximum efficiency versus F_2/ω. (c) Efficiency η_{ME} versus F_2/ω. (d) Tradeoff criterion $Q_{1,\mathrm{ME}}$ versus $\beta\omega$ for different F_2/ω. See text. The solid curves are those of nonlinear response (NLR), and the dashed curves pertain to linear response (LR). The parameters are $K = 0.1$, $\alpha = 5$, $\omega = 5\Delta_r$, and $\Delta_r = 1$. The parameter range covered by the plots is experimentally accessible in QPC transport experiments in the FQH regime [58,59].

So far, we have studied mean powers and power dispersion of the QBP converter in order Δ^2. Contributions of higher order in Δ^2 may become significant at sufficiently low T, depending on the parameters of the model. Starting out from the real-time version [43] of the Coulomb gas representation [63] of the perturbative series in Δ^2, we have calculated the Δ^4 terms of powers and variance numerically. These terms result from direct next-to-nearest-neighbor transitions in the TB lattice and coherent transport of two charges in the associated fermionic transport model. In addition to this, we have approximately taken into account all tunneling contributions of higher order in Δ^2 by summation of partial contributions in each order. The quality of this approximate treatment of the strong tunneling regime has been checked for the point $K = \frac{1}{2}$, for which all orders in Δ^2 can be summed exactly [43,57]. Formidable agreement down to very low temperatures has been found. The conclusions of the numerical analysis are that the higher-order tunneling terms yield marginal contributions up to inverse temperature $\beta\omega = 6$ for $\Delta_r = 1$, and the above weak-tunneling results are qualitatively correct down to much lower temperatures. Until now, reliable results in the asymptotic low temperature regime are missing. Nevertheless, it is rather unlikely that coherent tunneling transitions across many TB states will spoil the characteristics shown above.

IV. CONCLUSIONS

We have studied work-to-work conversion of a quantum Brownian particle in a TB lattice subjected to two isochromatic drives and coupled to a thermal bath with Ohmic spectral density. We have argued that this scenario can be experimentally realized and tested by a two-terminal setup of

a fractional quantum Hall bar with a quantum point contact. Analytic results in the linear response regime have been presented for mean power, efficiency, power fluctuations, and the tradeoff criterion. It has been shown that optimal performance at weak damping and low temperatures comes along with a clear undercut of the classical tradeoff bound. We have also focused on the performance in the regime of nonlinear response to driving with large amplitudes. It has been found that large power yield with low power fluctuations and with efficiency close to unity can be realized in a wide parameter range of the external drive. This reveals the hitherto mostly disregarded nonlinear response regime as a promising operation field for isothermal machines.

ACKNOWLEDGMENTS

We wish to thank Udo Seifert for stimulating discussions. M.C. acknowledges support from the project Quant-Eranet "SuperTop." M.S. thanks UniGE for financial support.

APPENDIX: POWER AND POWER FLUCTUATIONS

The Hamiltonian of the quantum Brownian particle (QBP) in a TB lattice with lattice spacing q_0, bilinearly coupled to a bath of harmonic oscillators and driven by two time-periodic forces of period $\mathcal{T}$, $\hbar\epsilon_1(t)/q_0$, and $\hbar\epsilon_2(t)/q_0$, is [43,57]

$$H(t) = H_{\rm TB} + H_{\rm RI} + H_{\rm ext}(t), \tag{A1}$$

where

$$H_{\rm TB} = -\frac{\hbar\Delta}{2}\sum_n (a_n^\dagger a_{n+1} + \text{H.c.}),$$

$$H_{\rm RI} = \sum_\alpha \left[\frac{p_\alpha^2}{2m_\alpha} + \frac{m_\alpha\omega_\alpha^2}{2}\left(x_\alpha - \frac{c_\alpha}{m_\alpha\omega_\alpha}q\right)^2\right], \tag{A2}$$

$$H_{\rm ext}(t) = -\hbar[\epsilon_1(t) + \epsilon_2(t)]q/q_0.$$

Here $q = q_0\sum_n a_n^\dagger a_n$, and $\hbar\Delta$ is the tunneling coupling energy of neighboring TB states. The spectral density of the bath coupling is $J(\omega) = \frac{\pi}{2}\sum_\alpha \frac{c_\alpha^2}{m_\alpha\omega_\alpha}\delta(\omega-\omega_\alpha)$. From now on we put $q_0 = \hbar = k_{\rm B} = 1$.

The power $P_i(t)$ $(i = 1, 2)$ for the drive $\epsilon_i(t)$ is related to the Brownian particle's velocity $\dot q(t)$ as

$$P_i(t) = \epsilon_i(t)\dot q(t). \tag{A3}$$

The TB representation of the average position of the Brownian particle is a perturbative series in Δ^2. It can be written as a grand-canonical sum of a one-dimensional gas of charges $e_j = \pm 1$ with complex interactions $e^{e_ie_j[W'(\tau_{ij})\pm iW''(\tau_{ij})]}$, where τ_{ij} is the distance of the charge pair [7,43,57]. The complex pair interaction $W(\tau) = W'(\tau) + iW''(\tau)$ includes all effects of the spectral bath coupling, and is defined as

$$W(\tau) = \frac{1}{\pi}\int_0^\infty d\omega \frac{J(\omega)}{\omega^2}\frac{\cosh\left[\omega\frac{\beta}{2}\right] - \cosh\left[\omega\left(\frac{\beta}{2} - i\tau\right)\right]}{\sinh\left[\omega\frac{\beta}{2}\right]}. \tag{A4}$$

For complex time $z = t - i\tau$, the equilibrium correlation function $W(z)$ is analytic in the strip $0 \geqslant \mathrm{Im}\, z > -\beta$ and satisfies

$$W(-z - i\beta) = W(z). \tag{A5}$$

In the weak tunneling limit, the position of the quantum Brownian particle at time t is

$$q(t) = \int_0^t dt_2 \int_0^{t_2} dt_1\, k_{\rm P}(t_2 - t_1)\sin[G(t_2, t_1)], \tag{A6}$$

where

$$k_{\rm P}(\tau) = \Delta^2 \sin[W''(\tau)]e^{-W'(\tau)} \tag{A7}$$

includes the bath correlations, and $G(t_2, t_1)$ is the total bias phase accumulated in the time interval extending from t_1 to t_2:

$$G(t_2, t_1) = \sum_{i=1,2}\int_{t_1}^{t_2} dt'\,\epsilon_i(t'). \tag{A8}$$

At times much larger than the decay time of $k_{\rm P}(\tau)$ (indicated by the overbar), the power $\overline{P}_i(t) = \epsilon_i(t)\bar q(t)$, $i = 1, 2$, is

$$\overline{P}_i(t) = \epsilon_i(t)\int_0^\infty d\tau\, k_{\rm P}(\tau)\sin[G(t, t-\tau)]. \tag{A9}$$

The function $\overline{P}_i(t)$ is a periodic function of t with period $\mathcal{T}$. The steady-state component $\langle P_i\rangle$ of $\overline{P}_i(t)$ is obtained upon taking the average over the period $\mathcal{T}$:

$$\langle P_i\rangle = \int_0^\infty d\tau\, k_{\rm P}(\tau)\int_0^{\mathcal{T}}\frac{dt}{\mathcal{T}}\epsilon_i(t)\sin[G(t, t-\tau)]. \tag{A10}$$

Consider next the power variance, which is defined as

$$D_i(t) = \frac{1}{t}\int_0^t dt_2\int_0^t dt_1\,\delta P_i(t_2)\delta P_i(t_1), \tag{A11}$$

where $\delta P_i(\tau) = P_i(\tau) - \overline{P}_i(\tau)$. At long times, we then have

$$\overline{D_i}(t) = \int_0^\infty d\tau\,[\,\overline{\delta P_i(t)\delta P_i(t-\tau)} + \overline{\delta P_i(t-\tau)\delta P_i(t)}\,], \tag{A12}$$

and, with the relation $P_i(t) = \epsilon_i(t)\dot q(t)$,

$$\overline{D_i}(t) = \int_0^\infty d\tau\,\epsilon_i(t)\epsilon_i(t-\tau)[\,\overline{\dot q(t)\dot q(t-\tau)} + \overline{\dot q(t-\tau)\dot q(t)} - 2\bar{\dot q}(t)\bar{\dot q}(t-\tau)]. \tag{A13}$$

From this, the steady-state component is found in order Δ^2 as

$$\langle D_i\rangle = \int_0^\infty d\tau\, k_{\rm D}(\tau)\int_0^{\mathcal{T}}\frac{dt}{\mathcal{T}}\epsilon_i(t)\epsilon_i(t-\tau)\cos[G(t, t-\tau)], \tag{A14}$$

where

$$k_{\rm D}(\tau) = \Delta^2\cos[W''(\tau)]\,e^{-W'(\tau)}. \tag{A15}$$

The property (A5) leads to the detailed balance relation [43]

$$\int_0^\infty d\tau\,\sin(\omega\tau)k_{\rm P}(\tau) = \coth\left(\frac{\omega\beta}{2}\right)\int_0^\infty d\tau\,\cos(\omega\tau)k_{\rm D}(\tau). \tag{A16}$$

The Ohmic spectral density of the coupling is $J(\omega) = 2\pi K\,\omega$, where K is the dimensionless coupling strength. Upon including modes above a cutoff frequency $\omega_{\rm c}$ in adiabatic approximation, we obtain from Eq. (A4) the analytic form

$$W(\tau) = 2K\ln[(\beta\omega_{\rm c}/\pi)\sinh(\pi|\tau|/\beta)] + i\pi K\,\mathrm{sgn}(\tau). \tag{A17}$$

With the dressed tunneling amplitude $\Delta_r = \Delta(\Delta/\omega_c)^{K/(1-K)}$, the functions (A7) and (A15) take in the range $\tau > 0$ the forms

$$k_P(\tau) = \Delta_r^2\left(\frac{\pi}{\beta\Delta_r}\right)^{2K}\frac{\sin(\pi K)}{\sinh[\pi\tau/\beta]^{2K}},$$
$$k_D(\tau) = \Delta_r^2\left(\frac{\pi}{\beta\Delta_r}\right)^{2K}\frac{\cos(\pi K)}{\sinh[\pi\tau/\beta]^{2K}}. \quad \text{(A18)}$$

1. Brownian duet

Consider mean power and power variance for isochromatic driving with an added multiple frequency term in the output channel, and a phase shift $\varphi = \arctan\alpha$ in the input channel:

$$\epsilon(t) = \epsilon_1(t) + \epsilon_2(t),$$
$$\epsilon_1(t) = F_1\,[\sin(\omega t) + \gamma_n \sin(n\omega t)], \quad \text{(A19)}$$
$$\epsilon_2(t) = F_2\cos(\omega t - \varphi).$$

With the drive (A19), the bias phase can be written as

$$G(t, t-\tau) = \frac{\mathcal{F}}{\omega}\{\cos[\omega(t-\tau)+\Phi] - \cos[\omega t + \Phi]\} + \frac{F_1}{n\omega}\gamma_n\{\cos[n\omega(t-\tau)] - \cos(n\omega t)\}, \quad \text{(A20)}$$

where $\mathcal{F} = \mathrm{sgn}\,(F_1 + F_2\sin\varphi)[F_1^2 + F_2^2 + 2F_1F_2\sin\varphi]^{1/2}$, and $\Phi = \arctan[F_2\cos\varphi/(F_1 + F_2\sin\varphi)]$. The bias phase factor

$$B(t, t-\tau) = e^{iG(t,t-\tau)} \quad \text{(A21)}$$

is a periodic function of time t. It can be written as the double Fourier series

$$B(t, t-\tau) = \sum_{k=-\infty}^{+\infty} J_k[A(\tau)]\,e^{-ik\omega\tau/2}e^{ik\Phi} \times \sum_{\ell=-\infty}^{+\infty} J_\ell[A_1(\tau)]\,e^{-i\ell n\omega\tau/2}\,e^{i(k+\ell n)\omega t}, \quad \text{(A22)}$$

where $J_k(z)$ is a Bessel function, and where

$$A(\tau) = 2\mathcal{F}\sin(\omega\tau/2)/\omega,$$
$$A_1(\tau) = 2F_1\gamma_n\sin(n\omega\tau/2)/(n\omega). \quad \text{(A23)}$$

With the Fourier series (A22), the time averages in Eqs. (A10) and (A14) are straightforward, yielding for $j = 1, 2$

$$\langle P_j\rangle = \int_0^\infty d\tau\, k_P(\tau)p_j(\tau),$$
$$\langle D_j\rangle = \int_0^\infty d\tau\, k_D(\tau)d_j(\tau). \quad \text{(A24)}$$

The functions $p_j(\tau)$ and $d_j(\tau)$ are defined by single infinite sums, in which the coefficients are products of two J-Bessel functions times phase factors. For $\gamma_n = 0$, we have $A_1(\tau) = 0$. Then the sums reduce to individual contributions. These are

$$p_1(\tau) = F_1J_1[A(\tau)]\cos(\Phi - \omega\tau/2),$$
$$p_2(\tau) = F_2J_1[A(\tau)]\,\sin(\Phi + \varphi - \omega\tau/2) \quad \text{(A25)}$$

and

$$d_1(\tau) = \frac{F_1^2}{2}[J_0[A(\tau)]\cos(\omega\tau) - J_2[A(\tau)]\cos(2\Phi)],$$
$$d_2(\tau) = \frac{F_2^2}{2}[J_0[A(\tau)]\cos(\omega\tau) + J_2[A(\tau)]\cos(2\Phi + 2\varphi)]. \quad \text{(A26)}$$

The expressions (A24) with (A25) and (A26) yield the expressions (8) and (9).

2. Linear response

In linear thermodynamics, the fluxes are linear in the forces, and the powers are quadratic forms of the forces, $\langle P_i\rangle = F_i\sum_{j=1,2}\mathcal{L}_{i,j}F_j$, where $\mathcal{L}$ is the Onsager matrix. Expanding the general expression (A9) up to terms quadratic in the forces F_1 and F_2, and taking the time average, we get

$$\langle P_i\rangle = \int_0^\infty d\tau\, k_P(\tau)\int_0^{\mathcal{T}}\frac{dt}{\mathcal{T}}\,\epsilon_i(t)G(t, t-\tau). \quad \text{(A27)}$$

From this, the Onsager matrix can be extracted as

$$\mathcal{L}_{i,j} = \int_0^\infty d\tau\, k_P(\tau)\int_0^{\mathcal{T}}\frac{dt}{\mathcal{T}}\,\frac{\epsilon_i(t)}{F_i}\int_{t-\tau}^{t}dt'\,\frac{\epsilon_j(t')}{F_j}. \quad \text{(A28)}$$

For the drive (A19), we get

$$\mathcal{L} = L_s(\omega)\begin{pmatrix}1+\rho_n & \frac{\alpha+\kappa}{\sqrt{1+\alpha^2}}\\ \frac{\alpha-\kappa}{\sqrt{1+\alpha^2}} & 1\end{pmatrix}, \quad \text{(A29)}$$

where $\kappa = L_c(\omega)/L_s(\omega)$ and $\rho_n = \gamma_n^2L_s(n\omega)/L_s(\omega)$. The functions $L_s(\omega)$ and $L_c(\omega)$ are

$$L_s(\omega) = \int_0^\infty d\tau\, k_P(\tau)\frac{\sin(\omega\tau)}{2\omega} \quad \text{(A30)}$$
$$L_c(\omega) = \int_0^\infty d\tau\, k_P(\tau)\frac{1-\cos(\omega\tau)}{2\omega}. \quad \text{(A31)}$$

The power variance in steady-state $\langle D_1\rangle$ to second order in the force is given by

$$\langle D_1\rangle = \int_0^\infty d\tau\, k_D(\tau)\int_0^{\mathcal{T}}\frac{dt}{\mathcal{T}}\epsilon_1(t)\epsilon_1(t-\tau) = \frac{F_1^2}{2}\int_0^\infty d\tau\, k_D(\tau)\,[\cos(\omega\tau) + \gamma_n^2\cos(n\omega\tau)]. \quad \text{(A32)}$$

Observing the detailed balance relation (A16), we finally obtain

$$\langle D_1\rangle = F_1^2\omega\coth(\beta\omega/2)\,\sigma_nL_s(\omega), \quad \text{(A33)}$$

where

$$\sigma_n = 1 + \gamma_n^2 n\,\frac{\coth(\beta n\omega/2)L_s(n\omega)}{\coth(\beta\omega/2)L_s(\omega)}. \quad \text{(A34)}$$

With the function (A17), the integrals (A30) and (A31) can be calculated in analytic form. The resulting expressions are

given in terms of Euler's function $\Gamma(z)$ as

$$L_s(\omega) = \frac{1}{2\beta\omega}\left(\frac{\beta\Delta_r}{2\pi}\right)^{2-2K} \sin(2\pi K)\Gamma(1-2K) \times \sinh\left(\frac{\beta\omega}{2}\right)\Gamma\left(K - i\frac{\beta\omega}{2\pi}\right)\Gamma\left(K + i\frac{\beta\omega}{2\pi}\right), \tag{A35}$$

$$L_c(\omega) = \frac{1}{\beta\omega}\left(\frac{\beta\Delta_r}{2\pi}\right)^{2-2K} \sin(\pi K)^2\Gamma(1-2K) \times \left[\Gamma(K)^2 - \Gamma\left(K - i\frac{\beta\omega}{2\pi}\right) \times \Gamma\left(K + i\frac{\beta\omega}{2\pi}\right)\cosh\left(\frac{\beta\omega}{2}\right)\right]. \tag{A36}$$

The ratio of these functions, $\kappa = L_c(\omega)/L_s(\omega)$, is

$$\kappa = \frac{\tan(\pi K)}{\sinh(\frac{\beta\omega}{2})}\left[\frac{\Gamma(K)^2}{\Gamma\left(K - i\frac{\beta\omega}{2\pi}\right)\Gamma\left(K + i\frac{\beta\omega}{2\pi}\right)} - \cosh\left(\frac{\beta\omega}{2}\right)\right]. \tag{A37}$$

a. Maximum output power

For the drive (A19), the maximum output power or yield is at

$$F_1 = F_{1,\mathrm{MP}} \equiv -\frac{\alpha+\kappa}{2\sqrt{1+\alpha^2}}\frac{F_2}{1+\rho_n}, \tag{A38}$$

yielding

$$\langle P_{1,\mathrm{MP}}\rangle = -(1+\rho_n)L_s(\omega)F_{1,\mathrm{MP}}^2. \tag{A39}$$

The two branches for the efficiency $\eta = |\langle P_1\rangle|/\langle P_2\rangle$ and the relative uncertainty $\Sigma = \sqrt{\langle D_1\rangle/\langle P_1\rangle^2}$ as functions of P^*, resulting from the condition $\langle P_1(F_1, F_2)\rangle/\langle P_{1,\mathrm{MP}}\rangle = P^*$, are

$$\eta_\pm = \frac{P^*}{2}\frac{X}{1+2/Y \mp \sqrt{1-P^*}},$$
$$\Sigma_{1,\pm} = \frac{2}{F_2}\frac{\sqrt{1+\alpha^2}}{\alpha+\kappa}\sqrt{\frac{\sigma_n\omega\coth(\beta\omega/2)}{L_s(\omega)}}\frac{1\pm\sqrt{1-P^*}}{P^*}, \tag{A40}$$

where

$$X = \alpha+\kappa)/(\alpha-\kappa),$$
$$Y = (\alpha^2-\kappa^2)/(1+r_n+\kappa^2), \tag{A41}$$
$$r_n = \gamma_n^2(1+\alpha^2)L_s(n\omega)/L_s(\omega).$$

In the absence of the multiple frequency drive, $\gamma_n = 0$, these forms reduce to the expressions (13) and (14).

b. Maximum efficiency

The efficiency η is maximal at $F_1 = F_{1,\mathrm{ME}}$, where

$$F_{1,\mathrm{ME}} = -\frac{\sqrt{1+\alpha^2}}{\alpha-\kappa}\left(1 - \sqrt{\frac{1+r_n+\alpha^2}{1+r_n+\kappa^2}}\right)F_2. \tag{A42}$$

It is given by

$$\eta_{\mathrm{ME}} = \frac{\sqrt{1+r_n+\alpha^2} - \sqrt{1+r_n+\kappa^2}}{\sqrt{1+r_n+\alpha^2} + \sqrt{1+r_n+\kappa^2}}\frac{\alpha+\kappa}{\alpha-\kappa}. \tag{A43}$$

The corresponding mean power and power fluctuations are

$$\langle P_{1,\mathrm{ME}}\rangle = -F_2^2\eta_{\mathrm{ME}}L_s(\omega)\sqrt{\frac{(1+r+\kappa^2)}{(1+\alpha^2)(1+\rho_n)}},$$
$$\Sigma_{1,\mathrm{ME}} = \sqrt{\sigma_n L_s(\omega)\,\omega\coth(\beta\omega/2)}\,F_{1,\mathrm{ME}}/\langle P_{1,\mathrm{ME}}\rangle. \tag{A44}$$

With the expressions (A43) and (A44), the tradeoff quantity

$$Q_{1,\mathrm{ME}} = \beta|\langle P_{1,\mathrm{ME}}\rangle|\,(1/\eta_{\mathrm{ME}} - 1)\,\Sigma_{1,\mathrm{ME}}^2 \tag{A45}$$

is found in analytic form as

$$Q_{1,\mathrm{ME}} = c(\beta\omega)\frac{\sigma_n}{\sqrt{1+\rho_n}}\frac{\sqrt{1+\alpha^2}}{(\alpha+\kappa)^2} \times \left(\frac{1+r_n-\alpha\kappa}{\sqrt{1+r_n+\kappa^2}} + \sqrt{1+r_n+\alpha^2}\right), \tag{A46}$$

where $c(x) = 2x\coth(x/2)$. In the absence of the multiple frequency term in the drive $\epsilon_1(t)$, $\gamma_n = 0$, we have $r_n = 0$ and $\sigma_n = 1$, and thus the expressions (A43) and (A46) reduce to the expressions (15) and (17).

In the asymptotic low temperature regime $\beta\omega \gg 1$, we obtain from (A35) and (A37)

$$L_s^{(\mathrm{as})}(\omega) = \frac{1}{4}\sin(2\pi K)\Gamma(1-2K)\left(\frac{\Delta_r}{\omega}\right)^{2-2K},$$
$$\kappa^{(\mathrm{as})} = \tan(\pi K)\left[\frac{\Gamma(K)^2}{\pi}\left(\frac{\beta\omega}{2\pi}\right)^{1-2K} - 1\right], \tag{A47}$$

and

$$\rho_n^{(\mathrm{as})} = \gamma_n^2/n^{2-2K},$$
$$\sigma_n^{(\mathrm{as})} = 1 + \gamma_n^2/n^{1-2K}, \tag{A48}$$
$$r_n^{(\mathrm{as})} = (1+\alpha^2)\gamma_n^2/n^{2-2K}.$$

Since $\kappa^{(\mathrm{as})}$ diverges for $K < 1/2$, as $\beta\to\infty$, whereas $\rho_n^{(\mathrm{as})}$, $\sigma_n^{(\mathrm{as})}$, and $r_n^{(\mathrm{as})}$ are temperature-independent in this limit, the qualitative behaviors of η_{ME} and $Q_{1,\mathrm{ME}}$ are independent of the coupling parameter γ_n. Altogether, the behaviors of efficiency, power fluctuations, and tradeoff $Q_{1,\mathrm{ME}}$ displayed in Figs. 1 and 2 change only marginally, when a multiple frequency contribution is added to the base-frequency term in the output $\epsilon_1(t)$.

When the multiple frequency contribution is added in the output channel, as in Eq. (A19), the element $\mathcal{L}_{1,1}$ of the Onsager matrix is modified by a factor $1+\rho_n$. If instead we had added a multiple frequency term in the input channel $\epsilon_2(t)$, the element $\mathcal{L}_{2,2}$ of the Onsager matrix would be changed by a factor $1+\rho_n$. With argumentation similar to that below Eq. (A49), one would find again that efficiency, power fluctuations, and tradeoff $Q_{1,\mathrm{ME}}$ change only marginally when a multiple frequency contribution is added to the base-frequency term in the input $\epsilon_2(t)$.

3. Mapping with quasiparticle tunneling through a quantum point contact (QPC) in a FQH system

Consider a fractional quantum Hall (FQH) bar (see Fig. 4) with Laughlin filling factor $\nu = 1/(2n+1)$ ($n \in \mathbb{N}$) described in hydrodynamical formulation [49] by the model Hamiltonian

$$H = H_0 + H_{\rm g} + H_{\rm T}, \tag{A49}$$

$$H_0 = \frac{\upsilon}{4\pi}\int_{-\infty}^{+\infty} dx\{[\partial_x\phi_{\rm R}(x)]^2 + [\partial_x\Phi_{\rm L}(x)]^2\}\,,$$

$$H_{\rm g} = -e\int_{-\infty}^{\infty} dx[\Theta(-x-d)V_1(t)\rho_{\rm R}(x) + \Theta(x-d)V_2(t)\rho_{\rm L}(x)],$$

$$H_{\rm T} = \Gamma_0\,[\Psi_{\rm R}^\dagger(0)\Psi_{\rm L}(0) + {\rm H.c.}]. \tag{A50}$$

Here, H_0 describes the chiral edge states with propagation direction R/L and velocity υ in terms of bosonic fields $\phi_{\rm R/L}$. The term $H_{\rm g}$ represents capacitive coupling of the densities $\rho_{\rm R/L}(x) = \mp\frac{\nu}{2\pi}\partial_x\phi_{\rm R/L}(x)$ with two voltage gates acting separately on the right- and left-moving excitations. The step functions $\Theta(\mp x - d)$ describe the case of very long contacts, which is in accordance with standard experimental setups [58,59]. The contacts are separated by distance $2d$. Weak backscattering transfer of quasiparticles between the two edges at the QPC located at $x = 0$ is described by the tunneling term $H_{\rm T}$. Here, $\Psi_{\rm R/L}(x) = (U_{\rm R/L}/\sqrt{2\pi a})\,e^{\pm i k_{\rm F} x}\,e^{-i\sqrt{\nu}\phi_{\rm R/L}(x)}$ is the quasiparticle annihilation operator, a is a cutoff length, U a Klein factor, and $k_{\rm F}$ is the Fermi momentum.

In the absence of the QPC, the currents at the terminals placed at $x = \pm d$ are the right-left-moving edge currents,

$$J_{x=\pm d}(t) = J_{0,{\rm R/L}}(t) = G_0\,V_{1/2}(t - 2d/\upsilon), \tag{A51}$$

where $G_0 = \frac{\nu e^2}{2\pi}$ is the universal quantum of conductance in the FQH regime. In the presence of the QPC, these current are modified by the backscattering current $J_{\rm bs}(t)$ of the quasiparticles as

$$J_{x=-d}(t) = J_{0,{\rm L}}(t) + J_{\rm bs}(t),$$
$$J_{x=d}(t) = J_{0,{\rm R}}(t) - J_{\rm bs}(t), \tag{A52}$$

and the associated powers are

$$P_{x=-d}(t) = V_1(t)[J_{0,{\rm L}}(t) + J_{\rm bs}(t)],$$
$$P_{x=d}(t) = V_2(t)[J_{0,{\rm R}}(t) - J_{\rm bs}(t)]. \tag{A53}$$

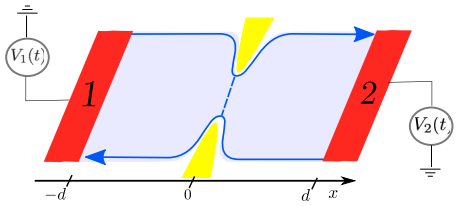

FIG. 4. Sketch of the two-terminal setup of a fractional quantum Hall bar with a quantum point contact (QPC). The QPC is placed at $x = 0$, and the two time-dependent voltages are applied at $x = -d$ and $x = d$.

The powers $P_{1/2}(t)$ resulting from backscattering alone are

$$P_1(t) \equiv P_{x=-d}(t) - V_1(t)J_{0,{\rm L}}(t) = V_1(t)J_{\rm bs}(t),$$
$$P_2(t) \equiv P_{x=d}(t) - V_2(t)J_{0,{\rm R}}(t) = -V_2(t)J_{\rm bs}(t). \tag{A54}$$

Following the analysis set out in Refs. [60,61], the backscattering current for weak quasiparticle tunneling is found as

$$J_{\rm bs}(t) = 2ive\left(\frac{\Gamma_0}{2\pi a}\right)^2\int_0^\infty d\tau\,\sin\left[\nu e\int_{t-\tau}^{t} dt'\,V_-(t')\right] \times\left(e^{2\nu\,\mathcal{G}(\tau)} - e^{2\nu\,\mathcal{G}(-\tau)}\right), \tag{A55}$$

where $V_-(t) = V_1(t) - V_2(t)$, and $\mathcal{G}(\tau)$ is the connected Green's function of the quasiparticle field $\phi(x,\tau)$ at $x = 0$, $\mathcal{G}(\tau) = \langle\phi_{\rm R/L}(0,\tau)\phi_{\rm R/L}(0,0)\rangle_{\rm c}$. Upon equating the filling factor ν with the Ohmic damping parameter K, and the length a with $\upsilon/\omega_{\rm c}$, there directly holds in the scaling limit the correspondence

$$2\nu\mathcal{G}(\tau) = -W(\tau), \tag{A56}$$

where $W(\tau)$ is the Ohmic bath correlation function (A17). With the correspondences $\epsilon_1(t) = \nu e\,V_1(t)$, $\epsilon_2(t) = -\nu e\,V_2(t)$, $G(t_2,t_1) = \nu e\int_{t_1}^{t_2} dt'\,[V_1(t') - V_2(t')]$, and with $\Delta = \frac{\Gamma_0}{\pi a}$, the mean backscattering current is found from Eq. (A55) as

$$J_{\rm bs}(t) = \nu e\int_0^\infty d\tau\,k_{\rm P}(\tau)\sin[G(t,t-\tau)]\,. \tag{A57}$$

Hence, time average of the powers $P_{1/2}(t)$ given in Eq. (A54) with the backscattering current (A57) directly yields the expression (A10) for $i = 1, 2$, which coincides with the expression (1). In accordance with this, the power fluctuation resulting from backscattering are found as given in Eq. (A14) with (A15), and in Eq. (2). Thus we have demonstrated complete correspondence in the scaling limit of the above QPC with the QBP system. The virtue of the QPC geometry is that powers running through the left and right terminals resulting from the backscattering current, and the associated power fluctuations, can be measured individually.

[1] U. Seifert, Rep. Prog. Phys. **75**, 126001 (2012).
[2] R. Kosloff, Entropy **15**, 2100 (2013).
[3] G. Benenti, G. Casati, K. Saito, and R. S. Whitney, Phys. Rep. **694**, 1 (2017).
[4] M. Esposito, U. Harbola, and S. Mukamel, Rev. Mod. Phys. **81**, 1665 (2009).
[5] M. Campisi, P. Hänggi, and P. Talkner, Rev. Mod. Phys. **83**, 771 (2011).
[6] A. Levy, R. Alicki, and R. Kosloff, Phys. Rev. E **85**, 061126 (2012).
[7] M. Carrega, P. Solinas, A. Braggio, M. Sassetti, and U. Weiss, New J. Phys. **17**, 045030 (2015).

[8] M. Carrega, P. Solinas, M. Sassetti, and U. Weiss, Phys. Rev. Lett. **116**, 240403 (2016).

[9] M. F. Ludovico, J. S. Lim, M. Moskalets, L. Arrachea, and D. Sanchez, Phys. Rev. B **89**, 161306(R) (2014).

[10] O. Maillet, P. A. Erdman, V. Cavina, B. Bhandari, E. T. Mannila, J. T. Peltonen, A. Mari, F. Taddei, C. Jarzynski, V. Giovannetti, and J. P. Pekola, Phys. Rev. Lett. **122**, 150604 (2019).

[11] P. Terren Alonso, J. Romero, and L. Arrachea, Phys. Rev. B **99**, 115424 (2019).

[12] F. Curzon and B. Ahlborn, Am. J. Phys. **43**, 22 (1975).

[13] R. S. Whitney, Phys. Rev. Lett. **112**, 130601 (2014).

[14] R. S. Whitney, Phys. Rev. B **91**, 115425 (2015).

[15] C. Van den Broeck, Phys. Rev. Lett. **95**, 190602 (2005).

[16] I. Goycuk and V. O. Kharchenko, Math. Modell. Nat. Phenom. **8**, 144 (2013).

[17] V. Holubec and A. Ryabov, Phys. Rev. E **92**, 052125 (2015).

[18] A. Ryabov and V. Holubec, Phys. Rev. E **93**, 050101(R) (2016).

[19] Y.-H. Ma, D. Xu, H. Dong, and C.-P. Sun, Phys. Rev. E **98**, 022133 (2018).

[20] M. Esposito, R. Kawai, K. Lindenberg, and C. Van den Broeck, Phys. Rev. Lett. **105**, 150603 (2010).

[21] V. Cavina, A. Mari, and V. Giovannetti, Phys. Rev. Lett. **119**, 050601 (2017).

[22] G. Benenti, K. Saito, and G. Casati, Phys. Rev. Lett. **106**, 230602 (2011).

[23] K. Proesmans, B. Cleuren, and C. Van den Broeck, Phys. Rev. Lett. **116**, 220601 (2016).

[24] K. Proesmans, Y. Dreher, M. Gavrilov, J. Bechhoefer, and C. Van den Broeck, Phys. Rev. X **6**, 041010 (2016).

[25] K. Proesmans and C. Van den Broeck, Chaos **27**, 104601 (2017).

[26] R. Luo, G. Benenti, G. Casati, and J. Wang, Phys. Rev. Lett. **121**, 080602 (2018).

[27] A. E. Allahverdyan, K. V. Hovhannisyan, A. V. Melkikh, and S. G. Gevorkian, Phys. Rev. Lett. **111**, 050601 (2013).

[28] M. Campisi and R. Fazio, Nat. Commun. **7**, 11895 (2016).

[29] V. Holubec and A. Ryabov, Phys. Rev. E **96**, 030102(R) (2017).

[30] M. Polettini and M. Esposito, Europhys. Lett. **118**, 40003 (2017).

[31] A. P. Solon and J. M. Horowitz, Phys. Rev. Lett. **120**, 180605 (2018).

[32] N. Shiraishi, K. Saito, and H. Tasaki, Phys. Rev. Lett. **117**, 190601 (2016).

[33] A. C. Barato and U. Seifert, Phys. Rev. Lett. **114**, 158101 (2015).

[34] J. M. Horowitz and T. R. Gingrich, Phys. Rev. E **96**, 020103(R) (2017).

[35] P. Pietzonka and U. Seifert, Phys. Rev. Lett. **120**, 190602 (2018).

[36] V. Holubec and A. Ryabov, Phys. Rev. Lett. **121**, 120601 (2018).

[37] N. Shiraishi and K. Saito, J. Stat. Phys. **174**, 433 (2019).

[38] A. C. Barato, R. Chetrite, A. Faggionato, and D. Gabrielli, New J. Phys. **20**, 103023 (2018).

[39] T. Koyuk, U. Seifert, and P. Pietzonka, J. Phys. A **52**, 02LT02 (2019).

[40] K. Brandner, T. Hanazato, and K. Saito, Phys. Rev. Lett. **120**, 090601 (2018).

[41] B. K. Agarwalla and D. Segal, Phys. Rev. B **98**, 155438 (2018).

[42] K. Ptaszynski, Phys. Rev. B **98**, 085425 (2018).

[43] U. Weiss, *Quantum Dissipative Systems*, 4th ed. (World Scientific, Singapore, 2012).

[44] G. Schön and A. D. Zaikin, Phys. Rep. **198**, 237 (1990).

[45] C. K. Andersen and K. Molmer, Phys. Rev. A **87**, 052119 (2013).

[46] G. Wendin, Rep. Prog. Phys. **80**, 106001 (2017).

[47] C. L. Kane and M. P. A. Fisher, Phys. Rev. Lett. **68**, 1220 (1992).

[48] J. Voit, Rep. Prog. Phys. **58**, 977 (1995).

[49] X. G. Wen, Phys. Rev. B **41**, 12838 (1990); **44**, 5708 (1991).

[50] C. L. Kane and M. P. A. Fisher, Phys. Rev. B **51**, 13449 (1995).

[51] T. Giamarchi, *Quantum Physics in One Dimension* (Oxford University Press, New York, 2004).

[52] D. Ferraro, M. Carrega, A. Braggio, and M. Sassetti, New J. Phys. **16**, 043018 (2014).

[53] G. Dolcetto, M. Sassetti, and T. L. Schmidt, Riv. Nuovo Cimento **39**, 113 (2016).

[54] H. Grabert and U. Weiss, Phys. Rev. Lett. **54**, 1605 (1985).

[55] M. P. A. Fisher and A. T. Dorsey, Phys. Rev. Lett. **54**, 1609 (1985).

[56] A. J. Leggett, S. Chakravarty, A. Dorsey, M. P. A. Fisher, A. Garg, and W. Zwerger, Rev. Mod. Phys. **59**, 1 (1987).

[57] M. Sassetti, M. Milch, and U. Weiss, Phys. Rev. A **46**, 4615 (1992); U. Weiss, M. Sassetti, T. Negele, and M. Wollensak, Z. Phys. B **84**, 471 (1991).

[58] J. Dubois, T. Jullien, F. Portier, P. Roche, A. Cavanna, Y. Jin, W. Wegscheider, P. Roulleau, and D. C. Glattli, Nature (London) **502**, 659 (2013).

[59] M. Kapfer, P. Roulleau, M. Santin, I. Farrer, D. A. Ritchie, and D. C. Glattli, Science **363**, 846 (2019).

[60] J. Rech, D. Ferraro, T. Jonckheere, L. Vannucci, M. Sassetti, and T. Martin, Phys. Rev. Lett. **118**, 076801 (2017).

[61] F. Ronetti, L. Vannucci, D. Ferraro, T. Jonckheere, J. Rech, T. Martin, and M. Sassetti, Phys. Rev. B **98**, 075401 (2018).

[62] The power law form (16) in the range $\beta\omega \gg 1$ originates from the short-time behavior $k_{\mathrm{P}}(\tau) \propto (\tau/\beta)^{-2K}$ of the expression (3) holding in the Ohmic scaling limit. Hence, Ohmic bath coupling is ultimately responsible for the possible undercut of the tradeoff bound observed in Figs. 2(b) and 3(d).

[63] G. Yuval and P. W. Anderson, Phys. Rev. B **1**, 1522 (1970).